Reducing computational workload from electrically large quadratic surface at high frequency

Yu Mao Wu[†] **Weng Cho Chew**[‡,†] and **Li Jun Jiang**[†]

[†]*Department of Electrical and Electronic Engineering, The University of Hong Kong, Pokfulam Road, Hong Kong, China, e-mail: yumaowu@hku.hk*

[‡] *Department of Electrical and Computer Engineering, University of Illinois at Urbana-Champaign, USA, 61801*

Abstract

In this paper, we propose a frequency independent approach, the numerical steepest descent path method, for computing the physical optics scattered electromagnetic field on the quadratic parabolic and saddle surfaces. Due to the highly oscillatory nature of the physical optics integral in the high frequency regime, the proposed method relies on deforming the integration path of the integral into the numerical steepest descent path on the complex plane. Furthermore, critical-point contributions which contain the stationary phase point, boundary resonance points, and vertex points, are comprehensively studied in terms of the numerical steepest descent path method. To illustrate the efficiency of the proposed method, some extensive numerical results for the physical optics integral defined on arbitrary lines, triangles and polygonal domains are demonstrated. Finally, numerical results on these quadratic surfaces illustrate that the proposed numerical steepest descent path method is frequency independent in computational cost and error controllable in accuracy.

1 Introduction

In electromagnetics (EM), when the product of the external wave frequency k and the size of the considered object L, i.e., kL ranges from tens

Pulsed Electromagnetic Fields: Their Potentialities, Computation and Evaluation
I. E. Lager and L. J. Jiang (Eds.).
doi: 10.3233/978-1-61499-230-1-41

to thousands, the analysis of the scattered EM field belongs to the high frequency regime problem. In this case, the classical *physical optics* (PO) current approximation [1, 2], has been accepted as an efficient way to capture the scattered EM field. Given the incident magnetic field $\boldsymbol{H}^{(i)}(\boldsymbol{r})$, the induced PO current on the surface of the considered object $\partial\Omega \subset \mathbb{R}^3$ is represented by

$$\boldsymbol{J}_{\mathrm{PO}}(\boldsymbol{r}) = \begin{cases} \hat{\boldsymbol{n}}(\boldsymbol{r}) \times \boldsymbol{H}^{(i)}(\boldsymbol{r}), & \boldsymbol{r} \in \partial\Omega_1 \\ 0, & \boldsymbol{r} \in \partial\Omega_2 \end{cases} \tag{1}$$

with $\partial\Omega = \partial\Omega_1 \bigcup \partial\Omega_2$, $\partial\Omega_1$ and $\partial\Omega_2$ are the lit and shadow regions of $\partial\Omega$, respectively. The resultant PO scattered electric field $\boldsymbol{E}^{(s)}(\boldsymbol{r})$ is

$$\boldsymbol{E}^{(s)}(\boldsymbol{r}) = \mathrm{i}\omega\mu \int_{\partial\Omega} \bar{\boldsymbol{G}}(\boldsymbol{r}, \boldsymbol{r'}) \cdot \boldsymbol{J}_{\mathrm{PO}}(\boldsymbol{r'})\, \mathrm{d}S(\boldsymbol{r'}) \tag{2}$$

where $\bar{\boldsymbol{G}}(\boldsymbol{r}, \boldsymbol{r'}) = \left(\bar{\boldsymbol{I}} + \frac{\nabla\nabla}{k^2}\right) \frac{\exp\left(\mathrm{i}k|\boldsymbol{r}-\boldsymbol{r'}|\right)}{4\pi|\boldsymbol{r}-\boldsymbol{r'}|}$ is the dyadic Green's function [3] for the electric field in an unbounded medium. Moreover, when kL is large enough, $\boldsymbol{E}^{(s)}(\boldsymbol{r})$ in (2) can be represented as three surface integrals [4]

$$I(\boldsymbol{r}) = \int_{\partial\Omega} s(\boldsymbol{r}, \boldsymbol{r'}) \exp\left[\mathrm{i}kv(\boldsymbol{r'})\right] \mathrm{d}S(\boldsymbol{r'}). \tag{3}$$

They are called the *surface PO integrals*. From the mathematical point of view, the PO integrand contains the slowly varying amplitude term $s(\boldsymbol{r}, \boldsymbol{r'})$, and the exponential of the phase function term $\exp\left[\mathrm{i}kv(\boldsymbol{r'})\right]$ giving the highly oscillatory behavior. It is quite changeling to efficiently calculate the PO integral in the high frequency regime.

In computational electromagnetic (CEM) community, the traditional method of moment method (MOM) [6] by Harrington via *surface integral equation* has a workload that grows dramatically with the working frequency as $O\left[(kL)^4\right]$. The efficient *multi level fast multipole algorithm* (MLFMA) developed by Chew [7] makes the computational effort reduce to $O\left[(kL)^2 \log(kL)\right]$. However, in the high frequency regime, the computational effort is still too high to afford. In contrast to these full wave methods like MOM and MLFMA, the PO approximation in (1) has been adopted as an efficient way to capture the scattered field from the large scale object [2,8]. The traditional *high frequency asymptotic* (HFA) approach [9–11], can provide the calculation of the PO scattered field with frequency independent workload. By the HFA method, the PO integrand is approximated by several leading terms. However, the generated PO results lose accuracy due to that kind of approximation, especially when kL is not extremely large but lies in the high frequency regime. The *numerical steepest descent path*

(NSDP) approach [13–16], provides an efficient way to evaluate the highly oscillatory PO integral. On invoking the NSDP method, the original PO *real* integration path is deformed into the *complex* NSDPs on the complex plane. In this manner, the PO integrands decay exponentially on the complex NSDPs, and it can be integrated with workload independent of frequency. In contrast to the HFA method, the only approximation done is the numerical integration of the exponential decay PO integrand. Hence, the proposed NSDP method improves the PO scattered field accuracy.

2 PO surface integral formulation

When a perfect conducting object is excited by an external source, the electromagnetic (EM) scattered fields can be expressed by the Stratton-Chu integral formulas [3]. For the observation point far away from the considered object, the far scattered electric field is expressed as

$$\boldsymbol{E}_s(\boldsymbol{r}) \approx -\frac{\mathrm{i}kZ_0 \exp(\mathrm{i}kr)}{4\pi r} \hat{\boldsymbol{r}} \times \hat{\boldsymbol{r}} \times \int_{\partial\Omega} \left[\hat{\boldsymbol{n}}(\boldsymbol{r}') \times \boldsymbol{H}(\boldsymbol{r}')\right] \exp\left(-\mathrm{i}k\hat{\boldsymbol{r}} \cdot \boldsymbol{r}'\right) \mathrm{d}S(\boldsymbol{r}') \tag{4}$$

where $\partial\Omega$ is the boundary of the object, k is the wave number outside Ω, ω is the angular frequency, $\boldsymbol{r}$ is the observation point with the amplitude r and unit vector $\hat{\boldsymbol{r}}$, $\boldsymbol{r}'$ is the surface point on $\partial\Omega$, $\hat{\boldsymbol{n}}(\boldsymbol{r}')$ is the outward unit normal vector of $\partial\Omega$, Z_0 is the free space intrinsic impedance constant. EM fields are time harmonic with the time dependence $\exp(-\mathrm{i}\omega t)$. For notation simplification, in the following, we still use $\partial\Omega$ to represent the lit region of the considered object. $\boldsymbol{H}^{(i)}(\boldsymbol{r}')$ is the incident magnetic field on $\partial\Omega$. In particular, we choose the plane incident wave

$$\boldsymbol{E}^{(i)}(\boldsymbol{r}) = \boldsymbol{E}_0^{(i)} \exp\left(\mathrm{i}k\hat{\boldsymbol{r}}^{(i)} \cdot \boldsymbol{r}\right) \tag{5}$$

$$\boldsymbol{H}^{(i)}(\boldsymbol{r}) = \frac{\hat{\boldsymbol{r}}^{(i)} \times \boldsymbol{E}_0^{(i)}}{Z_0} \exp\left(\mathrm{i}k\hat{\boldsymbol{r}}^{(i)} \cdot \boldsymbol{r}\right). \tag{6}$$

Then, after substituting (1), (5) and (6) into (4), the far scattered electric field can be represented by a surface integral

$$\boldsymbol{E}_s(\boldsymbol{r}) \approx \int_{\partial\Omega} \boldsymbol{s}_{\mathrm{bi}}(\boldsymbol{r}') \exp\left[\mathrm{i}kv_{\mathrm{bi}}(\boldsymbol{r}')\right] \mathrm{d}S(\boldsymbol{r}') \tag{7}$$

with

$$\boldsymbol{s}_{\mathrm{bi}}(\boldsymbol{r}') = -\frac{\mathrm{i}k\exp(\mathrm{i}kr)}{2\pi r}\,\hat{\boldsymbol{r}}\times\hat{\boldsymbol{r}}\times\left[\hat{\boldsymbol{n}}(\boldsymbol{r}')\times\hat{\boldsymbol{r}}^{(i)}\times\boldsymbol{E}_0^{(i)}\right] \tag{8}$$

$$v_{\mathrm{bi}}(\boldsymbol{r}') = \left(\hat{\boldsymbol{r}}^{(i)}-\hat{\boldsymbol{r}}\right)\cdot\boldsymbol{r}'. \tag{9}$$

The equation above is the bistatic scattered electric field under the PO approximation, which is called the PO integral. $\boldsymbol{E}_0^{(i)}$ in (5) and (6) is the incident electric polarization wave vector. In (8) and (9), $\boldsymbol{s}_{\mathrm{bi}}(\boldsymbol{r}')$ is the vector amplitude function which is usually slowly varying when the surface of the object is smooth. The exponential of the phase function term, $\exp\left[\mathrm{i}kv_{\mathrm{bi}}(\boldsymbol{r}')\right]$, will become highly oscillatory as the working frequency k increases.

In particular, for the monostatic case with $\hat{\boldsymbol{r}} = -\hat{\boldsymbol{r}}^{(i)}$, the PO surface integral in (7) can be represented as

$$\boldsymbol{E}_s(\boldsymbol{r}) \approx \boldsymbol{E}_0^{(i)}\tilde{I}_{\mathrm{mono}}, \tag{10}$$

with

$$\tilde{I}_{\mathrm{mono}} = \int_{\partial\Omega} s_{\mathrm{mono}}(\boldsymbol{r}')\exp\left[\mathrm{i}kv_{\mathrm{mono}}(\boldsymbol{r}')\right]\mathrm{d}S(\boldsymbol{r}'), \tag{11}$$

$$s_{\mathrm{mono}}(\boldsymbol{r}') = -\frac{\mathrm{i}k\exp(\mathrm{i}kr)}{2\pi r}\,\hat{\boldsymbol{r}}^{(i)}\cdot\hat{\boldsymbol{n}}(\boldsymbol{r}') \tag{12}$$

$$v_{\mathrm{mono}}(\boldsymbol{r}') = 2\hat{\boldsymbol{r}}^{(i)}\cdot\boldsymbol{r}'. \tag{13}$$

Comparing (12) and (13) with (8), the amplitude function now is simplified into a scalar function $s_{\mathrm{mono}}(\boldsymbol{r}')$. Furthermore, from (7) and (10), $\boldsymbol{E}_s(\boldsymbol{r})$ under the PO approximation for both the bistatic and monostatic cases takes the general form

$$\tilde{I} = \int_{\partial\Omega} s(\boldsymbol{r}')\exp\left[\mathrm{i}kv(\boldsymbol{r}')\right]\mathrm{d}S(\boldsymbol{r}'). \tag{14}$$

Here, the amplitude and phase terms are denoted as $s(\boldsymbol{r}')$ and $v(\boldsymbol{r}')$, respectively.

3 The quadratic polynomial approximation of the amplitude and phase functions

We assume that the surface of the object $\partial\Omega$ is governed by equation $z = f(x, y)$, and its projection onto the $x-y$ plane is $\partial\Omega_{xy}$. Then we use M triangular patches to discretize the domain $\partial\Omega_{xy}$, that is, $\triangle_1$, $\triangle_2$, $\cdots$, $\triangle_M$.

To capture the stationary phase and resonance points of the PO integrand in (3), we approximate the amplitude and phase functions by the second order polynomials on these triangular patches. Hence, the PO integral $\tilde{I}$ in (3) can be expressed as

$$\begin{aligned}\tilde{I} &= \int_{\partial\Omega_{xy}} \tilde{s}(x,y)\exp\left[\mathrm{i}k\tilde{v}(x,y)\right] t(x,y)\,\mathrm{d}x\mathrm{d}y \\ &= \sum_{n=1}^{M}\int_{\triangle_n} \tilde{d}(x,y)\exp\left[\mathrm{i}k\tilde{v}(x,y)\right]\mathrm{d}x\mathrm{d}y \simeq \sum_{n=1}^{M}\tilde{I}_n, \end{aligned} \tag{15}$$

Furthermore, after some affine transformations, the quadratic phase function $\tilde{v}_n(x,y)$ in each summation integral term in (15) has the simplified canonical form. In this manner, each summation integral term in (15) can be reformulated as

$$I_n = \int_{\triangle_n'} \tilde{p}_n(x',y')\exp\left\{\mathrm{i}k\left[\pm(x')^2 \pm (y')^2\right]\right\}\mathrm{d}x'\mathrm{d}y' \tag{16}$$

where

$$\tilde{p}_n(x',y') = \tilde{d}_n[x(x',y'),y(x',y')]\exp\left(\mathrm{i}k\tilde{G}_n|\boldsymbol{Q}_n|\right) \tag{17}$$

is also a second order polynomial in the $x'-y'$ coordinate system, and $\boldsymbol{Q}_n = \left[\frac{\partial(x,y)}{\partial(x',y')}\right]_{(\triangle_n\to\triangle_n')}$ is the Jacobi coordinate transform matrix between two coordinate systems $x-y$ and $x'-y'$. The above canonical expression (16) is valid for both monostatic and bistatic cases.

Due to the highly oscillatory behavior of the canonical form PO integral I_n in (16), if one evaluates it accurately by the direct numerical scheme, such as the adaptive Simpson's rule, the number of discretized triangle meshes in (15) shall increase as $M = M(k) \sim O(k^2)$. In the following, we will propose a NSDP method to k-independently evaluate the canonical PO integral I_n in (16).

4 The numerical steepest descent path method for the PO scattered field

We assume D as the trapezoidal domain, as shown in Fig. 1. We denote the $x-$values of vertex points $\boldsymbol{V}_1$ and $\boldsymbol{V}_2$ as L_1 and L_2, respectively. The governing line equation for edge $\boldsymbol{V}_3\boldsymbol{V}_4$ is $y = ax + b$, with $a > 0$. The amplitude phase function $p(x,y)$ has the similar form as $q(x,y)$ except with coefficients α_j instead, $j = 1,2,\ldots,6$.

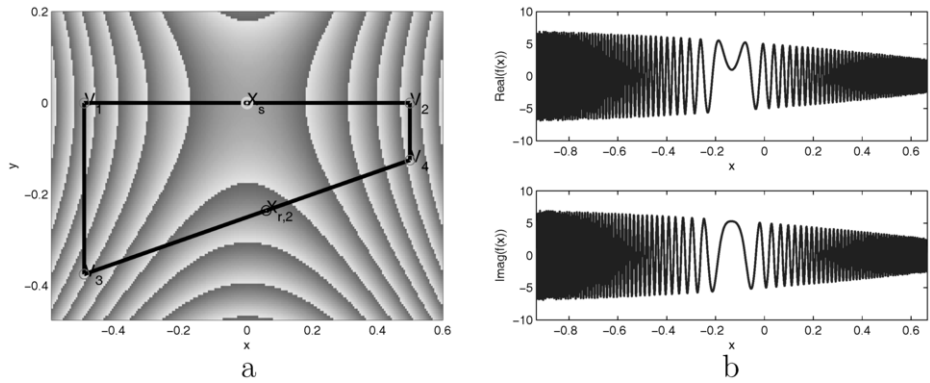

a b

Figure 1: (a) The integration domain is defined on $\boldsymbol{V}_1\boldsymbol{V}_2\boldsymbol{V}_3\boldsymbol{V}_4$, $[L_1, L_2] \times [ax + b, 0]$ for integrand $e^{\mathrm{i}k\left(-x^2+y^2\right)}$ with $a = 0.25$, $b = -0.5$; (b) highly oscillatory PO type integrand, $f(x) = (5 - 3x - x^2)e^{\mathrm{i}k(-x^2+(ax+b)^2)}$, with $k = 500$.

4.1 Reduction of the PO surface integral into highly oscillatory line integrals

$$\begin{aligned} I^{(a,b)} &= \int_{L_1}^{L_2} \int_{ax+b}^{0} p(x,y) \exp\left[\mathrm{i}k\left(-x^2+y^2\right)\right] \mathrm{d}y\mathrm{d}x \\ &= \int_{L_1}^{L_2} \left[J_2^{(0,0)}(x) - J_2^{(a,b)}(x)\right] \exp\left(-\mathrm{i}kx^2\right) \mathrm{d}x \end{aligned} \tag{18}$$

with $J_2^{(0,0)}(x)$ and $J_2^{(a,b)}(x)$ expressed as

$$J_2^{(0,0)}(x) = j_1(x) + j_2^{(0,0)}(x) \tag{19}$$

$$J_2^{(a,b)}(x) = j_1(x)\,\mathrm{erfc}\left[\sqrt{-\mathrm{i}k}(ax+b)\right] + j_2^{(a,b)}(x) \exp\left(\mathrm{i}k(ax+b)^2\right) \tag{20}$$

and

$$j_1(x) = -\frac{\sqrt{\pi}}{2\sqrt{-\mathrm{i}k}}\left(\alpha_1 + \alpha_2 x + \alpha_4 x^2 - \frac{\alpha_5}{2\mathrm{i}k}\right) \tag{21}$$

$$j_2^{(a,b)}(x) = \frac{\alpha_3 + \alpha_6 x + \alpha_5(ax+b)}{2\mathrm{i}k} \tag{22}$$

$$j_2^{(0,0)}(x) = \frac{\alpha_3 + \alpha_6 x}{2\mathrm{i}k}. \tag{23}$$

Hence, the original PO integral $I^{(a,b)}$ in (18) can be rewritten as

$$I^{(a,b)} = I_2^{(0,0)} - I_2^{(a,b)} \tag{24}$$

where

$$I_2^{(a,b)} = \int_{L_1}^{L_2} J_2^{(a,b)}(x) \exp\left(-\mathrm{i}kx^2\right) \mathrm{d}x \tag{25}$$

$$I_2^{(0,0)} = \int_{L_1}^{L_2} J_2^{(0,0)}(x) \exp\left(-\mathrm{i}kx^2\right) \mathrm{d}x. \tag{26}$$

Here, $I_2^{(a,b)}$ and $I_2^{(0,0)}$ are line integrals associated with edges $\boldsymbol{V}_1\boldsymbol{V}_2$ and $\boldsymbol{V}_3\boldsymbol{V}_4$, respectively.

4.2 Phase behavior of $I_2^{(a,b)}$ and its stationary phase point

As a result, the integrand $J_2^{(a,b)}(x)$ in (20) has the following asymptotic behavior

$$\begin{aligned} J_2^{(a,b)}(x) &= \begin{cases} j_1(x)\nu_1(x) \exp\left[\mathrm{i}k(ax+b)^2\right] \\ \quad +j_2^{(a,b)}(x) \exp\left[\mathrm{i}k(ax+b)^2\right], & x \in \mathcal{D}_1, \\ 2j_1(x) + j_1(x)\nu_2(x) \exp\left[\mathrm{i}k(ax+b)^2\right] \\ \quad +j_2^{(a,b)}(x) \exp\left[\mathrm{i}k(ax+b)^2\right], & x \in \mathcal{D}_2 \end{cases} \\ &= \begin{cases} \varsigma_1(x) \exp\left[\mathrm{i}k(ax+b)^2\right], & x \in \mathcal{D}_1, \\ 2j_1(x) + \varsigma_2(x) \exp\left[\mathrm{i}k(ax+b)^2\right], & x \in \mathcal{D}_2 \end{cases} \end{aligned} \tag{27}$$

with $\varsigma_1(x)$, $\varsigma_2(x)$ denoted as slowly varying functions. $\mathcal{D}_1$ and $\mathcal{D}_2$ are the domains separated by the *Stokes' line* on the complex plane, with the expressions

$$l_{\mathrm{Stokes}}(x) : \mathrm{Im}(x) = -\mathrm{Re}(x) - \frac{b}{a} \tag{28}$$

$$\mathcal{D}_1 := a\left[\mathrm{Re}(x) + \mathrm{Im}(x)\right] + b > 0 \tag{29}$$

$$\mathcal{D}_2 := a\left[\mathrm{Re}(x) + \mathrm{Im}(x)\right] + b < 0. \tag{30}$$

For the case $x \in \mathcal{D}_2$ in (27), the first term $2j_1(x)$ comes from the Stokes' phenomenon of the complementary error function.

After substituting (27) into (25), we get two phase function terms for $I_2^{(a,b)}$. They are

$$g_1(x) = -x^2 + (ax+b)^2 \tag{31}$$

$$g_2(x) = -x^2. \tag{32}$$

The above equations indicate that the Stokes' phenomenon of complementary error function makes the phase behaviors of the PO integrand $I_2^{(a,b)}$ be discontinuous.

4.3 Numerical steepest descent paths for $I_2^{(a,b)}$

Firstly, we consider the first phase function $g_1(x)$ of $I_2^{(a,b)}$ in (31) and (32). Physically, there may exist a point x_s, at which the phase behavior of $g_1(x)$ is different from others. It is called the *stationary phase point* (SPP). SPP corresponds to the point at which the specular reflection occurs in the high frequency ray physics regime. Mathematically, the SPP x_s satisfies the condition $g_1'(x_s) = 0$. As a result, we have the mathematical expression of x_s as

$$x_s = \begin{cases} \frac{ab}{1-a^2}, & |a| \neq 1 \\ \text{no stationary phase point}, & |a| = 1 \end{cases} \tag{33}$$

Now we see the term $\exp[\mathrm{i}kg_1(x)]$ in the PO integrand

$$\begin{aligned} \exp[\mathrm{i}kg_1(x)] &= \exp\left(\mathrm{i}k\left\{\mathrm{Re}[g_1(x)] + \mathrm{i}\,\mathrm{Im}[g_1(x)]\right\}\right) \\ &= \exp\left\{-k\,\mathrm{Im}[g_1(x)] + \mathrm{i}k\,\mathrm{Re}[g_1(x)]\right\}. \end{aligned} \tag{34}$$

The NSDP method relies on the transformation of the above highly oscillatory functions to exponential decay functions on the complex plane.

To achieve this, for a starting point L_*, we define a complex path function $x = \varphi_{L_*}(p)$ as that in [3], satisfying the following identity

$$-\varphi_{L_*}(p)^2 + [a\varphi_{L_*}(p) + b]^2 = -L_*^2 + (aL_* + b)^2 + ip^l, \tag{35}$$

with $l = 1$ for integration end points L_1 and L_2, and $l = 2$ for the SPP x_s. After substituting L_1, L_2 and x_s into (35), the corresponding NSDPs are

$$\varphi_{L_m}(p) = \begin{cases} \frac{\mathrm{sgn}(L_m')}{\sqrt{a^2-1}}\sqrt{{L_m'}^2 + \mathrm{i}p} + x_s, & |a| > 1, \quad p \in [0, \infty) \\ \frac{\mathrm{sgn}(L_m')}{\sqrt{1-a^2}}\sqrt{{L_m'}^2 - \mathrm{i}p} + x_s, & |a| < 1, \quad p \in [0, \infty) \\ L_m + \frac{\mathrm{i}p}{2ab}, & |a| = 1, \quad p \in [0, \infty) \end{cases} \tag{36}$$

$$\varphi_{x_s}(p) = \begin{cases} \frac{p\sqrt{\mathrm{i}}}{\sqrt{|1-a^2|}} + x_s, & |a| > 1, \quad p \in (-\infty, \infty) \\ \frac{p\sqrt{-\mathrm{i}}}{\sqrt{|1-a^2|}} + x_s, & |a| > 1, \quad p \in (-\infty, \infty) \\ \text{no NSDP}, & |a| = 1, \quad p \in (-\infty, \infty) \end{cases} \tag{37}$$

Here,

$$L_m' = \sqrt{|1-a^2|}\left(L_m - \frac{ab}{1-a^2}\right) = \sqrt{|1-a^2|}(L_m - x_s), \quad m = 1, 2. \tag{38}$$

In Fig. 2, we demonstrate the diagrams of the NSDPs expressed in (36) and (37), with cases $a > 1$ and $a = 1$. Possible cases of NSDP occur when a

changes to the negative sign. However, for the brevity of this paper, we skip those cases here.

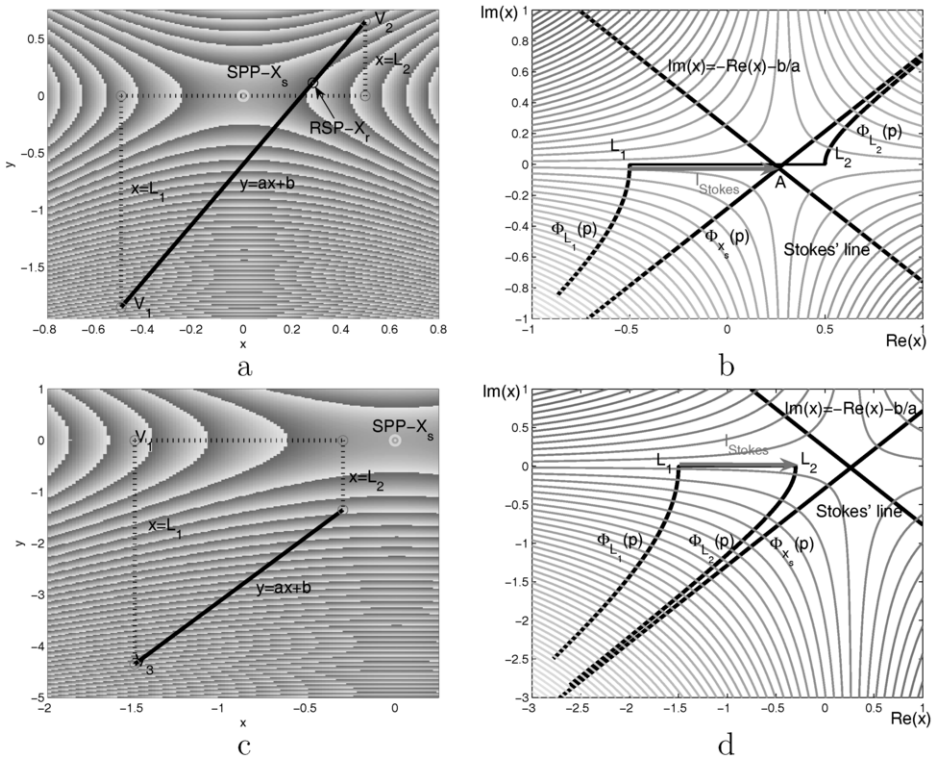

Figure 2: Sub-figures (a) and (b): $I_2^{(a,b)}$ defined on the integration domain $[L_1, L_2]$ with $L_1 < x_s < L_2$, and its numerical steepest descent paths $\varphi_{L_1}(p) \bigcup \varphi_{x_s}(p) \bigcup \varphi_{L_2}(p)$; sub-figures (c) and (d): $I_2^{(a,b)}$ defined on the integration domain $[L_1, L_2]$ with $x_s > L_2$, and its numerical steepest descent paths $\varphi_{L_1}(p) \bigcup \varphi_{L_2}(p)$.

With the above expressions for NSDPs, we give the following main theorem in this paper.

Theorem 4.1 (Frequency independent theorem by the NSDP method)**.** *The highly oscillatory integrand of* $I_2^{(a,b)}$ *in* (25), (26), *i.e.,* $J_2^{(a,b)}(x) \exp\left(-\mathrm{i}kx^2\right)$ *defined on the real integration domain* $[L_1, L_2]$ *can be transformed to that defined on several complex NSDPs on the complex plane, denoted as* $\varphi_{\mathrm{NSDPs}}(p)$*, that takes the formulation*

$$\varphi_{\mathrm{NSDPs}}(p) = \begin{cases} \varphi_{L_1}(p) \bigcup \varphi_{x_s}(p) \bigcup \varphi_{L_2}(p), & L_1 < x_s < L_2 \\ \varphi_{L_1}(p) \bigcup \varphi_{L_2}(p), & L_2 < x_s \end{cases} \tag{39}$$

with these two cases shown in Fig. 2. Then, $I_2^{(a,b)}$ *takes the formulation*

$$I_2^{(a,b)} = \begin{cases} I_{2,L_1}^{(a,b)} + I_{2,x_s}^{(a,b)} - I_{2,L_2}^{(a,b)} + K_2(\boldsymbol{A}) - K_2(L_1,0), & L_1 < x_s < L_2 \\ I_{2,L_1}^{(a,b)} - I_{2,L_2}^{(a,b)} + K_2(L_2,0) - K_2(L_1,0), & L_2 < x_s \end{cases}. \quad (40)$$

Here, $I_{2,L_1}^{(a,b)}$, $I_{2,L_2}^{(a,b)}$ *and* $I_{2,x_s}^{(a,b)}$ *are integrals with exponential decay integrands defined on* $\varphi_{L_1}(p)$, $\varphi_{L_2}(p)$ *and* $\varphi_{x_s}(p)$, *respectively. The complex point* $\boldsymbol{A}$ *corresponds to the intersection point in Fig. 2, and* $K_2(x)$ *is the primitive function of kernel* $2j_1(x)\exp\left(-\mathrm{i}kx^2\right)$ *in* (21), *with the formula*

$$K_2(x) = \left(\frac{\pi}{2k}\alpha_1 + \frac{\pi}{4\mathrm{i}k^2}\alpha_4 - \frac{\pi}{4\mathrm{i}k^2}\alpha_5\right)\mathrm{erfc}\left(\sqrt{\mathrm{i}k}\,x\right) + \left(\frac{\sqrt{\pi}}{2\mathrm{i}k\sqrt{-ik}}\alpha_2 + \frac{\sqrt{\pi}x}{2\mathrm{i}k\sqrt{-ik}}\alpha_4\right)\exp\left(-\mathrm{i}kx^2\right). \quad (41)$$

Furthermore, on invoking the Gauss-Laguerre quadrature rule, the PO integrand $J_2^{(a,b)}(x)\exp\left(-\mathrm{i}kx^2\right)$ *defined on* $\varphi_{\mathrm{NSDPs}}(p)$ *can be integrated with workload independent of frequency* k, *as* $k \gg 1$.

The detailed proof is given in [17].

5 Numerical results

To illustrate the efficiency of the proposed NSDP method, first, we conduct some numerical experiments for the PO line integral $I_2^{(a,b)}$. Next, we

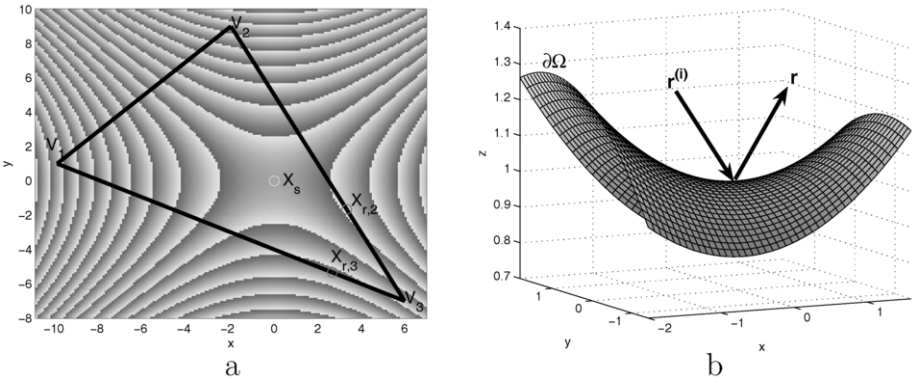

Figure 3: (a) PO surface integral $I_{\triangle_1}$, defined on the triangular patch–Δ_1; (b) the electromagnetic wave impinges on the quadratic saddle surface $\partial\Omega$, governed by equation $z = f(x,y)$.

extend the PO surface integral on the triangular patch. Finally, the RCS values of the PO scattered electric field on the saddle surface are generated via the proposed NSDP method.

5.1 PO surface integral on the triangular patch

In this subsection, we consider the triangular patch $\triangle_1$, as shown in Fig. 3. The critical points in $\triangle_1$ contain the SPP $\boldsymbol{X}_s$, two RSPs $\boldsymbol{X}_{r,m}$ and three vertex points $\boldsymbol{V}_n$, $m = 2, 3$, $n = 1, 2, 3$.

In contrast to the HFA method, Fig. 4 depicts that the PO results by the NSDP method can be significantly improved by one to two orders when $k \in [10, 100]$, as expressed by $E_{\Delta_1}^{(\mathrm{NSDP})}(k)$ and $E_{\Delta_1}^{(\mathrm{HFA})}(k)$. Meanwhile, the computational effort for the PO integral by the NSDP method is also $O(1)$.

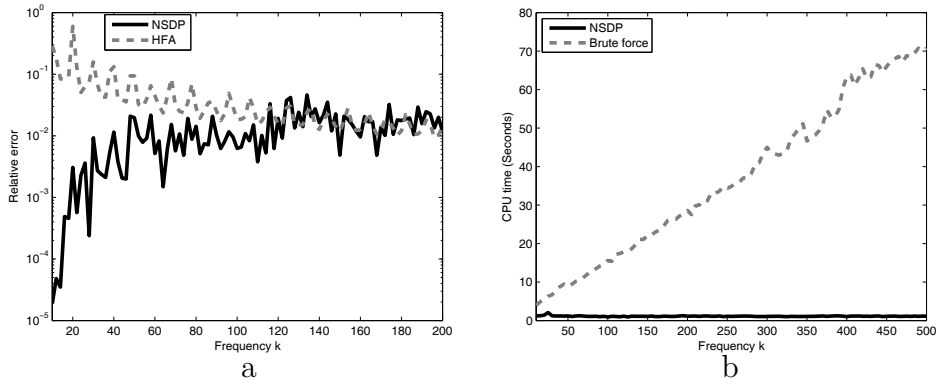

Figure 4: (a) The relative errors of the PO results by using the NSDP and HFA methods relative to the BF method on Δ_1, denoted by $E_{\Delta_1}^{(\mathrm{NSDP})}(k)$ and $E_{\Delta_1}^{(\mathrm{HFA})}(k)$; (b) CPU time comparisons by using NSDP and BF methods.

5.2 PO scattered field on the saddle surface

Finally, we apply the NSDP method to analyze the PO scattered field on the saddle surface in Fig. 3. The incident wave propagates along $\hat{\boldsymbol{r}}^{(i)} = \left[0.5, 0.5, -\sqrt{2}/2\right]$ direction, and the observation point is set along the direction $\hat{\boldsymbol{r}} = \left[\sqrt{2}/4, \sqrt{6}/4, \sqrt{2}/2\right]$.

Figure 5 gives comparisons of the errors of $\boldsymbol{E}_s(\boldsymbol{r})$ produced by NSDP and HFA methods relative to the BF method. Compared with the HFA method, the advantage on improving the scattered electric field accuracy by the NSDP method is again confirmed in Fig. 5.

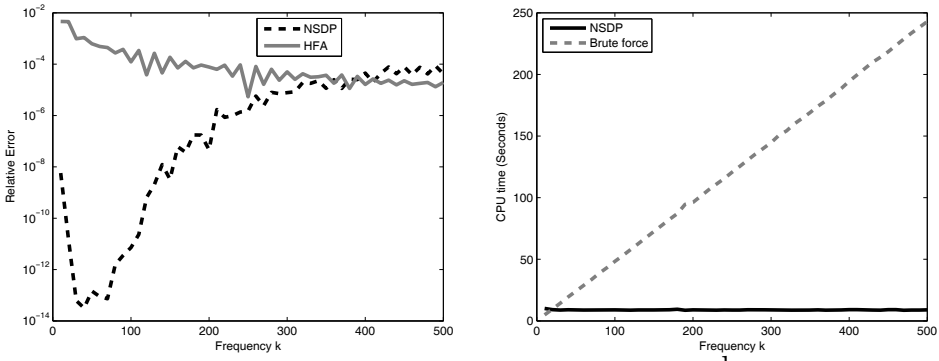

Figure 5: (a) The relative errors of the bistatic scattered electric field $\boldsymbol{E}_s(\boldsymbol{r})$ results by using NSDP and HFA methods relative to the BF method on the saddle surface; (b) comparisons of the CPU time (second unit) for the PO scattered electric field by using NSDP and BF methods.

On invoking the NSDP method, the various critical-point contributions to $\boldsymbol{E}_s(\boldsymbol{r})$ are compared in Fig. 6. Also, we see that the SPP point contribution dominates $\boldsymbol{E}_s(\boldsymbol{r})$ when k is large. Again, Fig. 5 demonstrates the frequency independent computational effort for the scattered electric field. Finally, we apply the NSDP method to calculate the bistatic RCS values of $\boldsymbol{E}_s(\boldsymbol{r})$, which are in good agreement with the results generated by the BF method.

In summary, the proposed NSDP method for calculating the PO scattered field on the quadratic saddle surface is frequency independent and error controllable.

6 Conclusion

In this paper, we propose the NSDP method to calculate the scattered field on the quadratic saddle surface in the high frequency regime. The scattered electric field can be reduced to several highly oscillatory PO surface integrals. By applying the NSDP method, high frequency critical-point contributions are rigorously expressed on these NSDPs. Finally, extensive numerical experiments are given to show the efficiency of the NSDP method. In conclusion, the NSDP method for calculating the electric scattered field on the quadratic saddle surface is frequency independent and error controllable.

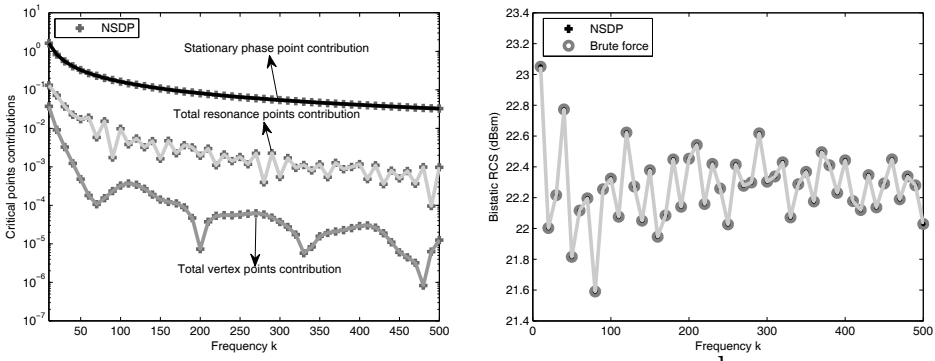

Figure 6: (a) Critical points contributions to $\boldsymbol{E}_s(\boldsymbol{r})$ in (7) in terms of the NSDP method; (b) comparisons of the RCS (dBsm unit) values of the PO scattered electric field on the saddle surface by using NSDP and BF methods.

Acknowledgment

This work was supported in part by the Research Grants Council of Hong Kong (GRF 711511, 713011, and 712612), HKU Small Project Funding(201007176196), HKU Seed funding (201102160033), HKU UDF-CSE grant, and in part by the University Grants Council of Hong Kong (Contract No. AoE/P-04/08).

Bibliography

[1] H. M. Macdonald, "The effect produced by an obstacle on a train of electric waves," *Phil. Trans. Royal Soc. London, Series A, Math. Phys. Sci.*, no. 212, pp. 299–337, 1913.

[2] P. Y. Ufimtsev, "New insight into the classical macdonald physical optics approximation," *IEEE Antennas Propag. Mag.*, vol. 50, no. 3, pp. 11–20, June 2008.

[3] W. C. Chew, *Waves and Fields in Inhomogeneous Media*, New York: IEEE Press, 1995.

[4] J. A. Kong, *Electromagnetic Wave Theory*, Cambridge, MA: EMW Publishing, 2000.

[5] W. C. Chew, M. S. Tong, and B. Hu, *Integral Equations Methods for Electromagnetic and Elastic Waves*, Morgan and Claypool, 2008.

[6] R. Harrington, *Field Computation by Moment Method*, New York: Macmillan, 1968.

[7] J. M. Song, C. C. Lu, and W. C. Chew, "Multilevel fast multipole algorithm for electromagnetic scattering by large complex objects," *IEEE Trans. Antennas Propag.*, vol. 45, no. 10, pp. 1488–1493, Oct. 2009.

[8] A. C. Ludwig, "Computation of radiation patterns involving numerical double integration," *IEEE Trans. Antennas Propag.*, vol. 16, no. 6, pp. 767–769, Nov. 1968.

[9] S. W. Lee and G. A. Deschamps, "A uniform asymptotic theory of electromagnetic diffraction by a curved wedge," *IEEE Trans. Antennas Propag.*, vol. 24, no. 1, pp. 25–34, Jan. 1976.

[10] G. Carluccio, M. Albani, and P. H. Pathak, "Uniform asymptotic evaluation of surface integrals with polygonal integration domains in terms of UTD transition functions," *IEEE Trans. Antennas Propag.*, vol. 58, no. 4, pp. 1155–1163, April, 2010.

[11] R. Wong, *Asymptotic Approximations of Integrals*, New York: SIAM, 2001.

[12] M. Abramowitz and I. A. Stegun, *Handbook of Mathematical Functions*, Mineola, NY: Dover Publications Inc., 1972.

[13] Y. M. Wu, L. J. Jiang, and W. C. Chew, "An efficient method for computing highly oscillatory physical optics integral," *Progress In Electromagnetics Research (PIER)* vol. 127, pp. 211–257, April, 2012.

[14] Y. M. Wu, L. J. Jiang, and W. C. Chew, "An efficient method for computing highly oscillatory physical optics integral," in *Proc. IEEE International Symposium on Antennas and Propagation and USNC-URSI National Radio Science Meeting* pp. 1–2, Chicago, USA, July, 2012.

[15] Y. M. Wu, L. J. Jiang, W. E. I. Sha, and W. C. Chew, "The numerical steepest descent path method for calculating physical optics integrals on smooth conducting surfaces," *IEEE Trans. Antennas Propag.*, in revision.

[16] Y. M. Wu, L. J. Jiang, and W. C. Chew, "Computing highly oscillatory physical optics integral on the polygonal domain by an efficient numerical steepest descent path method," *J. Comput. Phys.*, November 24, 2012, [Online]. Available: dx.doi.org/10.1016/j.jcp.2012.10.052.

[17] Y. M. Wu, W. C. Chew, and L. J. Jiang, "A frequency independent method for computing high frequency physics optics scattered electromagnetic fields on saddle surfaces," *SIAM Journal on Scientific Computing*, submitted.